Advances in Differential Equations and Control Processes 2025, 32(4), 3693.
doi: https://doi.org/10.59400/adecp3693

Article

Bifurcation and chaos analysis of a gear-shaft-bearing system considering tooth-bearing backlash nonlinearity and time-varying mesh stiffness

Wei Liu[1], Ying Cui[1], Qiang Wang[1,*], Hanlong Cai[2], Weimin Ding[2]

[1] College of Automobile and Traffic Engineering, Heilongjiang Institute of Technology, Harbin 150050, China
[2] Ningbo Donly Transmission Equipment Co., LTD, Ningbo 315000, China
*** Corresponding author:** Qiang Wang, wangqiang@hljit.edu.cn

CITATION

Liu W, Cui Y, Wang Q, et al. Bifurcation and chaos analysis of a gear-shaft-bearing system considering tooth-bearing backlash nonlinearity and time-varying mesh stiffness. Advances in Differential Equations and Control Processes. 2025; 32(4): 3693. https://doi.org/10.59400/adecp3693

ARTICLE INFO

Received: 10 September 2025
Revised: 23 September 2025
Accepted: 5 October 2025
Available online: 23 October 2025

Abstract: The bifurcation and chaos of gear-shaft-bearing system considering tooth-bearing backlash nonlinearity and time-varying mesh stiffness (TVMS) are investigated through employing shafting element method. In our previous work, the dynamic system merely considered the simple nonlinear backlash and completely ignored the case that tooth-bearing backlash were introduced simultaneously. This work primarily concentrates on the investigation of nonlinear dynamics of gear-shaft-bearing system with tooth-bearing backlash. Initially, TVMS is calculated and simulated to validate Y.Cai result. The coupling relationship for the tooth backlash, TVMS and time-varying center distance is taken into account. Accordingly, the expression of TVMS considering tooth backlash and time-varying center distance is decuced theroetically. Based on the shaft element method, the whole gear dynamic model is established mathematically with the help of the shaft element, gear mesh element and bearing element. Bifurcation diagrams of the system are investigated and compared for three cases, i.e., only tooth backlash, no coupling backlash and coupling backlash. Furthermore, time-domain responses, phase diagrams, and Poincare maps of central components with different speed conditions are analyzed. Ultimately, the illustrative parametric studies are further scrutinized to exhibit the nonlinear dynamics. The results show that chaotic motion region of gear system becomes wider while coupling the tooth-bearing backlash nonlinearity. With the speed condition increase, the gear system exhibits significant nonlinear behavior, i.e., periodic motion and chaotic motion. This work is extremely helpful for the optimization design and vibration reduction of gear system.

Keywords: gear transmission system; multiple backlash; nonlinear; bifurcation; TVMS

1. Introduction

Gear systems are extensively applied to many transmission fields such as automobile and ship gearbox because of their large transmission ratio and strong load capacity. In practical systems where vibration and noise problem of gear transmission system is a critical concern, the nonlinear backlash is meaningful and should be considered, particularly for multiple backlash case. Actually, gear systems are affected by many excitation forces such as transmission error, TVMS and backlash, which lead to the reduction of performance and reliability of gearbox. Investigation of nonlinear dynamic is extremely valuable for the structural design and vibration reduction of gear systems.

Nonlinear dynamics of gear transmission system have been thoroughly

investigated by many literature [1–4]. Cao et al. [5] aimed to suppress the torsional vibration of gear-shafting system by introducing NES device. Ren et al. [6] analyzed the nonlinear dynamics of a coupled lateral-torsional spur gear with eccentricity through employing lumped parameter method. Influence of speed condition, TVMS and multiple clearance on the nonlinear dynamics is also discussed. Hu et al. [7] analyzed the nonlinear response of gear system including uncertain interval shaft misalignment. Wei et al. [8] presented a theoretical and experimental investigation on the nonlinear behavior of helical gearbox with modification, and the experimental dynamic responses verified the correctness of theoretical predictions. In order to better present the nonlinear dynamics, Shi et al. [9] established a novel gear-bearing dynamic model to investigate the multi-meshing-state. Xiang [10] proposed a nonlinear multistage gear transmission system with multi-clearance and analyzed the nonlinear responses by introducing the backlash bifurcation parameter. Pan et al. [11] qualitatively studied the bifurcation and chaos motion of gear-shaft-bearing system considering tooth contact temperature and random excitation. The effect of temperature, tooth backlash and random excitation on nonlinear dynamics was discussed. Zhang et al. [12] analyzed the nonlinear dynamics of gear rotor bearing systems with coupled multi-clearance. The above-mentioned gear dynamic model cannot accurately show the effect of shaft, bearing and housing on the nonlinear behavior. To introduce the shaft, bearing and housing into gear system, recently, this work has been further extended to a new gear-rotor-bearing model with multi-clearance. Tatsuhito and Kensho [13] theoretically studied the resonance curves and bifurcation diagrams of gear pair with shafts. Wang et al. [14] established a nonlinear dynamic model of a fixed-axis spur planetary gear-rotor-bearing system considering time-varying meshing stiffness, tooth face friction, transmission errors, gear backlash and bearing clearance. Sun et al. [15] gave a more comprehensive nonlinear dynamic model of gear-rotor-bearing system including thermal related material properties, backlash, friction and gyroscopic effect, and compared the dynamic response of this system under different steady-state temperature fields. Cheon [16] extended the nonlinear dynamic model of gear transmission system considering both hydrodynamic lubrication and sliding friction. Lu et al. [17] studied the nonlinear characteristics of gear-rotor-bearing system with mesh force and misalignment spline coupling.

The above-mentioned studies exhibit the nonlinear behavior of gear system, gear-shaft-bearing system and gear-rotor system, merely considering the tooth-bearing backlash. However, researches on coupling effect for tooth-bearing backlash are rare. Actually, the jump of the bearing backlash can cause the variation of center distance, leading to the variation of meshing position of tooth clearance. On the basis of our previous published literature [18], the objectives of this manuscript are to explore the nonlinear dynamics and coupling effect of gear-shaft-bearing system considering tooth-bearing backlash nonlinearity and TVMS.

Accordingly, this work constructs a novel nonlinear model of gear-shaft-bearing system considering tooth-bearing backlash nonlinearity and TVMS to predict the nonlinear response. TVMS formula associated with tooth-bearing backlash is derived. Bifurcation and chaos of gear-shaft-bearing system are analyzed. Influence of speed

condition, backlash effect and TVMS on the bifurcation and chaos is investigated. This work is significant for the structural design and vibration reduction of gear systems.

2. Gear-shaft-bearing model

A comprehensive gear-shaft-bearing model with shaft element, mesh element and bearing element is presented in **Figure 1**. The gear-shaft-bearing model is simplified as a limited element discrete model with 4 bearing units, 1 gear mesh unit and 40 shaft units [8,19]. **Figure 2** shows the finite element discrete condition of gear-shaft-bearing system. According to calculation accuracy requirement, the whole system can be divided into multiple discrete body.

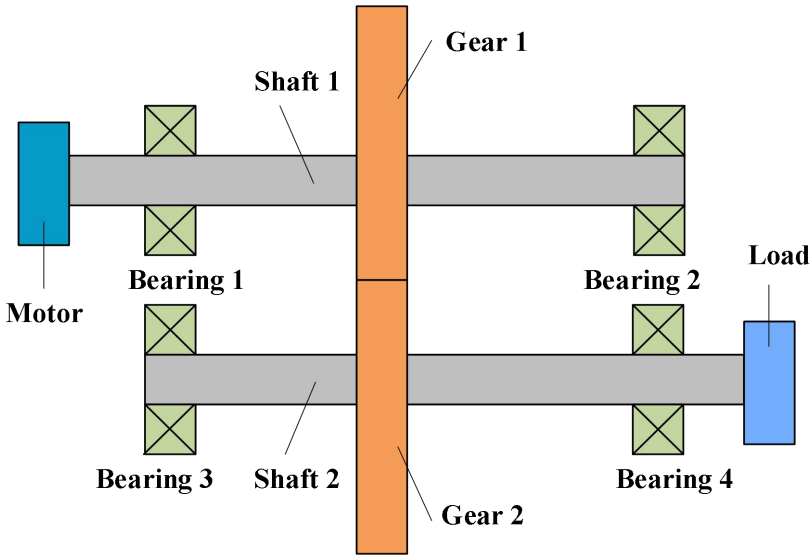

Figure 1. Gear-shaft-bearing model.

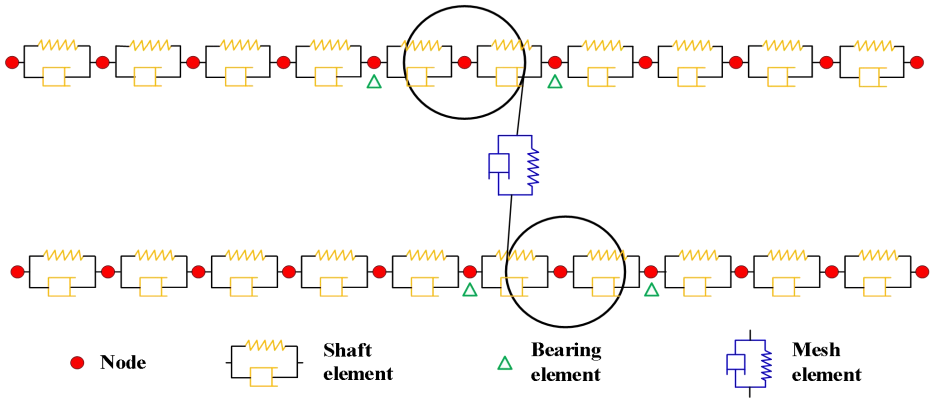

Figure 2. Finite element discrete model.

2.1. Shaft element

In the gear system, shaft is primarily employed to transmit rotation speed and torsional force. In order to achieve an accurate motion condition, in this analysis, the equivalent dynamic model of the shaft element is adopted here by using Timoshenko beam theory. Motion equation can be expressed as:

$$\boldsymbol{M}_s\ddot{\boldsymbol{q}}_s + \boldsymbol{C}_s\dot{\boldsymbol{q}}_s + \boldsymbol{K}_s\boldsymbol{q}_s = \boldsymbol{0} \tag{1}$$

where damping matrix can be calculated based on the Rayleigh formula $\boldsymbol{C}_{\mathrm{s}} = \alpha \boldsymbol{M}_{\mathrm{s}} + \beta \boldsymbol{K}_{\mathrm{s}}$. Mass matrix $\boldsymbol{M}_s$ and stiffness matrix $\boldsymbol{K}_{\mathrm{s}}$ can be found in Page 195 in David's paper [20].

2.2. Gear meshing element

In practical meshing process, tooth backlash of gear system can generate derivations, leading to the variation of the meshing characteristic. In this section, the relational formula of tooth backlash including center distance and motion equation of gear system are derived mathematically to capture the coupling relationship. For this purpose, gear meshing element is simplified as two rigid disks connected by spring k_m and damper c_m. The gear meshing element with 12-DOF is established, as depicted in **Figure 3a**. Each gear is taken into account as a rigid body with 3-DOF transnational and torsional motion and the generalized coordinates can be expressed as $q_{12} = [x_1, y_2, z_3, \theta_{x_1}, \theta_{y_1}, z_1, x_2, y_2, z_2, \theta_{i_2}, \theta_{j_2}, \theta_2]^{\mathrm{T}}$. Gears 1-2 denote driving and driven wheels. The relative deformations of gear system along the oxy plane are illustrated in **Figure 3b**. Dashed line denotes installation location while solid line denotes relative location. Time-varying center distance $l(t)$, pressure angle $\alpha(t)$ and position angle $\varphi(t)$ can be achieved based on the following relationships

$$\begin{cases} l(t) = \sqrt{[l_0 \cos\phi_0 + (x_2(t) - x_1(t))]^2 + [l_0 \sin\phi_0 + (y_2(t) - y_1(t))]^2} \\ \alpha(t) = \cos^{-1}\left(\frac{r_{b1}+r_{b2}}{l(t)}\right) \\ \varphi(t) = \alpha(t) - \tan^{-1}\left(\frac{l_0 \cos\phi_0 + (x_2(t) - x_1(t))}{l_0 \sin\phi_0 + (y_2(t) - y_1(t))}\right) \end{cases} \tag{2}$$

where l_0 denotes center distance. ϕ_0 denotes relative position angle. r_{b1}, r_{b2} denote base circle radii.

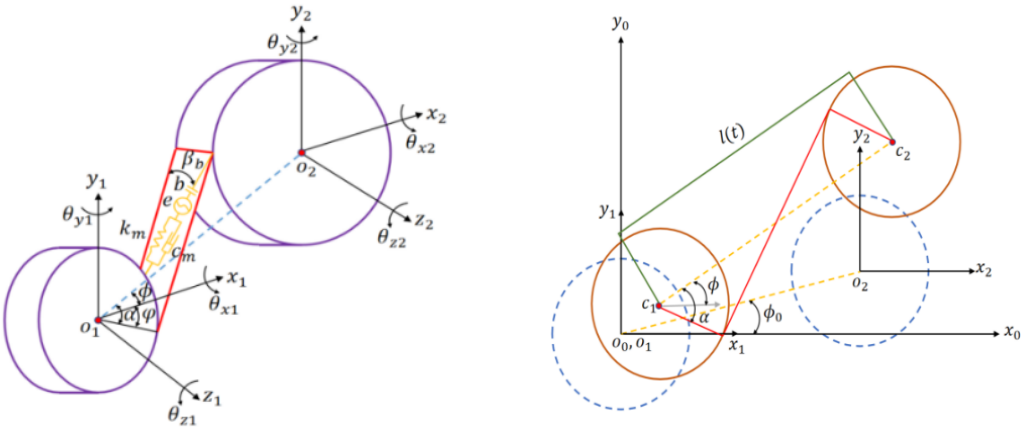

(**a**) Center distance of theroetical meshing gear pair (**b**) Center distance of practial meshing gear pair

Figure 3. Meshing element of gear pair.

Displacement vector of gear pair along the meshing direction is defined as V performed in Equation (3). δ denotes the relative total deformation described in Equation (4). $e_m(t)$ denotes the transmission error expressed in Equation (5). Here, e_m denotes the fluctuation amplitude. φ_1 denotes the initial phase. ω_m denotes meshing

frequency $\omega_m = \omega_1 z_1 = \omega_2 z_2$.

$$\begin{gathered} V = [\cos\beta_b \sin\varphi(t), \pm\cos\beta_b \cos\varphi(t), \sin\beta_b, \\ \mp r_b \sin\beta_b \sin\varphi(t), -r_{b1} \sin\beta_b \cos\varphi(t), \pm r_{b1} \cos\beta_b, \\ -\cos\beta_b \sin\varphi(t), \mp\cos\beta_b \cos\varphi(t), -\sin\beta_b, \\ \mp r_{b2} \sin\beta_b \sin\varphi(t), -r_{b2} \sin\beta_b \cos\varphi(t), \pm r_{b2} \cos\beta_b] \end{gathered} \tag{3}$$

$$\delta = Vq_{12} - e_m(t) \tag{4}$$

$$e_m(t) = e_m \sin(\omega_m t + \varphi_1) \tag{5}$$

Direction of meshing surface varies with the change of steering of driving wheel, leading to a positive or negative symbol in front of the parameters. Additionally, variation of rotation direction is also affected by the position angle $\varphi(t)$.

$$\varphi(t) = \alpha(t) \mp \phi(t) \tag{6}$$

Elastic meshing force can be described as:

$$F_d = k_m(t) f(\delta) + c_m \frac{df(\delta)}{dt} \tag{7}$$

where $k_m(t)$ denotes TVMS. c_m denotes damping. $f(\delta)$ denotes nonlinear displacement function including backlash nonlinearity described in Equation (8). Taking the helical gear as an example, meshing force of tooth surface can be decomposed into three directions: radial, axial and tangential. The meshing force is described as:

$$f(\delta) = \begin{cases} \delta - b & \delta \geq b \\ 0 & |\delta| < b \\ \delta + b & \delta \leq -b \end{cases} \tag{8}$$

$$\begin{cases} F_x = F_d \cos\beta_b \sin\varphi \\ F_y = F_d \cos\beta_b \cos\varphi \\ F_z = F_d \sin\beta_b \end{cases} \tag{9}$$

Actually, dynamic backlash can be divided into two categories: constant backlash and time-varying backlash. Here, backlash caused by tooth thickness deviation and center distance installment error is called constant backlash described by $2b_0$. Backlash caused by center distance variation due to gear geometric eccentricity or bearing elastic deformation is called time-varying backlash described by $b(t)$. In this work, they are taken into account simultaneously. The time-varying backlash is proposed as below [21]:

$$\Delta b = 2(r_{b1} + r_{b2})(inv(\alpha(t) - inv(\alpha_0)) \tag{10}$$

The whole dynamic tooth backlash is described as:

$$b(t) = 2b_0 + \Delta b \tag{11}$$

Therefore, deformation function along the meshing line can be modified as:

$$f(\delta)=\begin{cases}\delta-b(t)/2 & \delta\geq b(t)/2\\ 0 & |\delta|<b(t)/2\\ \delta+b(t)/2 & \delta\leq -b(t)/2\end{cases} \tag{12}$$

Dynamic equation of gear meshing element is proposed as:

$$\begin{cases}m_1\ddot{x}_1+F_x=0\\ m_1\ddot{y}_1\pm F_y=0\\ m_1\ddot{z}_1\mp F_z=0\\ I_{x1}\ddot{\theta}_{x1}+F_z\sin\varphi r_{b1}=0\\ I_{y1}\ddot{\theta}_{y1}\pm F_z\cos\varphi r_{b1}=0\\ I_{z1}\ddot{\theta}_{z1}\pm F_d\cos\beta_b r_{b1}=0\end{cases}\text{(driving gear)}\quad\begin{cases}m_2\ddot{x}_2-F_x=0\\ m_2\ddot{y}_2\mp F_y=0\\ m_2\ddot{z}_2\pm F_z=0\\ I_{x2}\ddot{\theta}_{x2}+F_z\sin\varphi r_{b2}=0\\ I_{y2}\ddot{\theta}_{y2}\pm F_z\cos\varphi r_{b2}=0\\ I_{z2}\ddot{\theta}_{z2}\pm F_d\cos\beta_b r_{b2}=0\end{cases}\text{(driven gear)} \tag{13}$$

where m_1, m_2 denote mass. I_x, I_y, I_z denote rotational inertia along x, y and z axis. Damping formula denotes $c_m=2\xi r_{m0}\sqrt{\bar{k}_m/(1/m_{e1}+1/m_{e2})}$. Here, ξ denotes damping ratio. m_{e1}, m_{e2} denote equivalent mass of gears 1–2, respectively.

The tooth of gear will go through the process of contact-disengagement-contact due to the dynamic backlash effect, leading to a significant nonlinear behavior. In order to discriminate the contact and disengagement, a step separation function $r_m(\delta)$ is introduced. Defining the meshing case, one obtains $|\delta|>b(t)/2$, $r_m(\delta)=1$. Defining the tooth separation case, one obtains $|\delta|\leq b(t)/2$, $r_m(\delta)=0$. Expression of step separation function can be described as:

$$r_m(\delta)=\begin{cases}0 & |\delta|\leq b(t)/2\\ 1 & |\delta|>b(t)/2\end{cases} \tag{14}$$

After considering the nonlinearity of tooth separation caused by dynamic backlash, the TVMS formula is described as:

$$k_m(t)=k_m(t)r_m(\delta)=\begin{cases}k_m(t) & |\delta|>b(t)/2\\ 0 & |\delta|\leq b(t)/2\end{cases} \tag{15}$$

Substituting Equation (2), Equation (4), Equation (11) into Equation (15), TVMS can be rearranged as Equation (16). It can be observed from Equation (16) that $k_m(t)$ is no longer a variable parameter related to backlash b_0. It is also influenced by the center distance $l(t)$. Hence, the TVMS formula is given by:

$$k_m(t)=\begin{cases}k_m(t) & |\delta|>b_0+(r_{b1}+r_{b2})(inv(\cos(\frac{r_{b1}+r_{b2}}{l(t)}))-inv(\alpha_0))\\ 0 & |\delta|\leq b_0+(r_{b1}+r_{b2})(inv(\cos(\frac{r_{b1}+r_{b2}}{l(t)}))-inv(\alpha_0))\end{cases} \tag{16}$$

Substituting Equations (2)–(9) into Equation (12), one obtains:

$$\boldsymbol{M}_m\ddot{\boldsymbol{q}}_{12}+\boldsymbol{C}_m\dot{\boldsymbol{q}}_{12}+\boldsymbol{K}_m\boldsymbol{q}_{12}=\boldsymbol{F}_e \tag{17}$$

2.3. Bearing element

The specific expression of stiffness matrix of bearing element is:

$$\boldsymbol{K}_b = \begin{bmatrix} k_{xx} & 0 & 0 & 0 & 0 & 0 \\ 0 & k_{yy} & 0 & 0 & 0 & 0 \\ 0 & 0 & k_{zz} & 0 & 0 & 0 \\ 0 & 0 & 0 & k_{\theta_{xx}} & 0 & 0 \\ 0 & 0 & 0 & 0 & k_{\theta_{yy}} & 0 \\ 0 & 0 & 0 & 0 & 0 & 0 \end{bmatrix} \tag{18}$$

where k_{xx}, k_{yy} denote radial bearing stiffness. k_{zz} denotes axial bearing stiffness. $k_{\theta_{xx}}$, $k_{\theta_{yy}}$ denote bearing torsional stiffness.

Dynamic equation of bearing element is proposed as:

$$\boldsymbol{M}_i\ddot{\boldsymbol{q}}_i + \boldsymbol{C}_b\dot{\boldsymbol{q}}_i + \boldsymbol{K}_b\boldsymbol{q}_i = 0 \tag{19}$$

where $\boldsymbol{M}_i$ denotes mass matrix. $\boldsymbol{C}_b$ and $\boldsymbol{K}_b$ denote damping and stiffness matrix. $\boldsymbol{q}_i$ denotes displacement vector in the generalized coordinate system.

$$\boldsymbol{q}_i = \left[f(x_i)\ , f(y_i)\ , f(z_i)\ ,\ \theta_{xi}\ ,\ \theta_{yi}\ ,\ \theta_{zi}\right]^T \tag{20}$$

Here, $f(x_i)$, $f(y_i)$, $f(z_i)$ are the nonlinear backlash functions of bearing separation. The specific formulas are expressed as:

$$\begin{gathered} f(x_i) = \begin{cases} x_i - b_1 & x_i > b_1 \\ 0 & |x_i| \le b_1 \\ x_i + b_1 & x_i < -b_1 \end{cases} \quad f(y_i) = \begin{cases} y_i - b_1 & y_i > b_1 \\ 0 & |y_i| \le b_1 \\ y_i + b_1 & y_i < -b_1 \end{cases} \\ f(z_i) = \begin{cases} z_i - b_2 & z_i > b_2 \\ 0 & |z_i| \le b_2 \\ z_i + b_2 & z_i < -b_2 \end{cases}, (i = 1, 2, 3) \end{gathered} \tag{21}$$

where b_1 denotes radial bearing backlash. b_2 denotes axial bearing backlash.

2.4. Equation of motion

The whole dynamic equation of gear-shaft-bearing model is devoloped based on the aforementioned formulation i.e., shaft element, meshing element and bearing element. Combining these element matrices, the whole dynamic equation can be integrated as:

$$\boldsymbol{M}\ddot{q}(t) + \boldsymbol{C}\dot{q}(t) + \boldsymbol{K}(t)f(q(t)) = \boldsymbol{P}_0 + \boldsymbol{F}_e(t) \tag{22}$$

where $\boldsymbol{M}$, $\boldsymbol{C}$, $\boldsymbol{K}(t)$ denote mass, damping and stiffness matrix. $\boldsymbol{q}(t)$ denotes displacement vector. $f(\boldsymbol{q}(t))$ denotes deformation function for meshing backlash and bearing backlash. $\boldsymbol{P}_0$ force vector. $\boldsymbol{F}_e(t)$ excitation vector generated by transmission error. Compared with traditional model, the established gear-shaft-bearing model provides a basic model and will be employed for the following coupling study, particularly for the tooth-bearing backlash.

3. Nonlinear dynamics analysis

For a gear pair, the nonlinear dynamics are affected by meshing stiffness, tooth backlash and bearing backlash while are meshing at required speed condition. In this section, TVMS of gear-shaft-bearing system is validated through comparing theoretical results with those available data in literature. Dynamic performance of gear system is investigated for the case of only considering tooth backlash, not coupling tooth-bearing backlash, coupling tooth-bearing backlash.

3.1. Meshing stiffness verification

TVMS is one of the most critical parameters for gear-shaft-bearing system. Accurate calculation of TVMS is the basis for the investigation of nonlinear response. In this work, the dynamic equations of gear-shaft-bearing system are calculated by adopting MATLAB software. The parameters of gear element are tabulated in **Table 1**. The mean value and amplitude value of meshing stiffness are selected as 6×10^8 N/m and 6×10^7 N/m. The values of transmission error and backlash are selected as 14.1 um and 12 um. Transmission error and TVMS curves are described in **Figures 4** and **5**.

To examine the feasibility of Y.Cai result, in this particular case, the theoretical simulation is carried out. **Figure 6** indicates that the present result is basically consistent with those in Cai's findings [22]. This verification can provide excellent basis for the investigation of nonlinear dynamics.

Table 1. Parameters of gear element.

Parameters	Driving gear	Driven gear
Tooth number	23	57
Module (mm)	3.85	3.85
Pressure angle (°)	25	25
Helical angle (°)	15	15
Tooth width (mm)	35	35

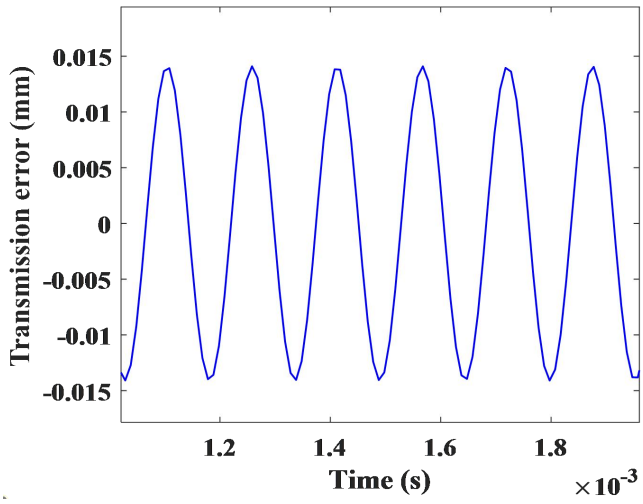

Figure 4. Transmission error curve.

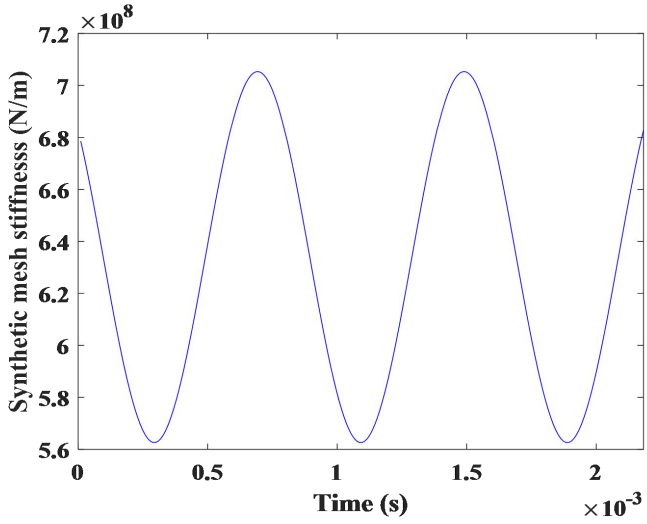

Figure 5. TVMS curve.

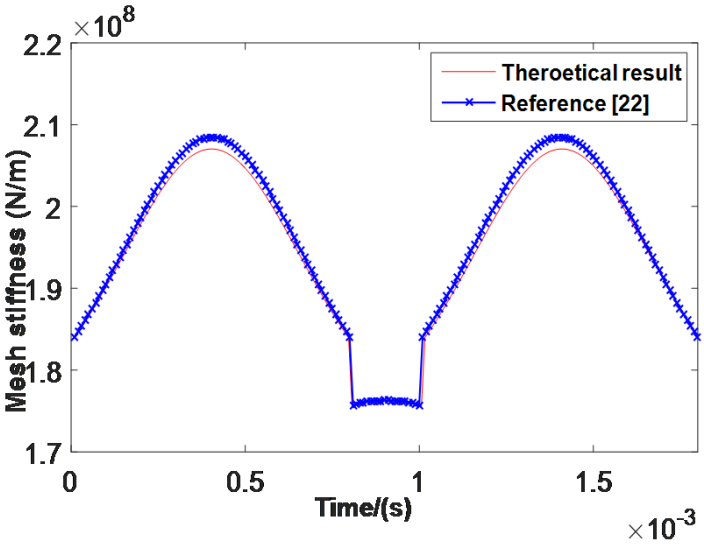

Figure 6. TVME curve comparison.

3.2. Nonlinear response comparisons

In this section, the coupling relationship for the tooth backlash, TVMS and time-varying center distance is further taken into account. Accordingly, the expression of TVMS considering tooth backlash and time-varying center distance can be achieved. Parameters of shaft and bearing elements have been tabulated in **Table 2** and **3**. The bifurcation curves of torsional displacement of gear-shaft-bearing model can be smoothly plotted through substituting TVMS formula into the whole dynamic equation, as depicted in **Figures 7–9**.

Table 2. Parameters of shaft element.

Length L (mm)	Outer diameter D (mm)	Inner diameter d (mm)	Young modulus E (Pa)	Density ρ (kg/m^3)	Poisson σ
100	50	40	2.09×10^{11}	7850	0.03

Table 3. Parameters of bearing element.

Transverse stiffness (N/m)	Torsional stiffness (N/m)	Damping (N·s/m)	Backlash (um)
$k_{xx} = k_{yy} = 5 \times 10^7, k_{zz} = 1 \times 10^7$	$k_{\theta x \theta x} = k_{\theta y \theta y} = 5 \times 10^5, k_{\theta z \theta z} = 0$	1000	6

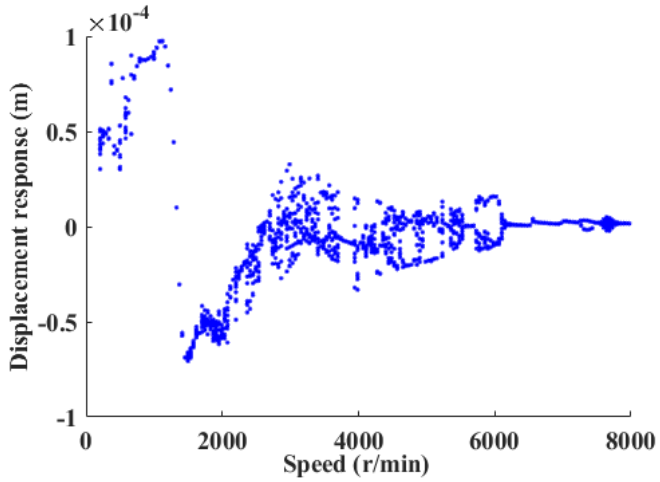

Figure 7. Bifurcation diagram with backlash.

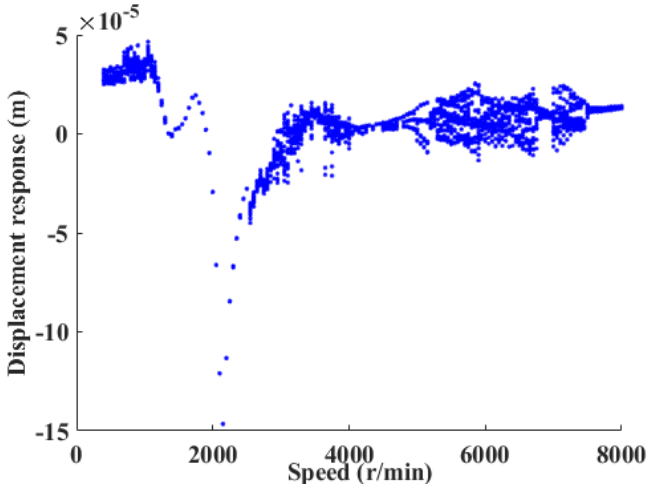

Figure 8. Bifurcation diagram without coupling backlash.

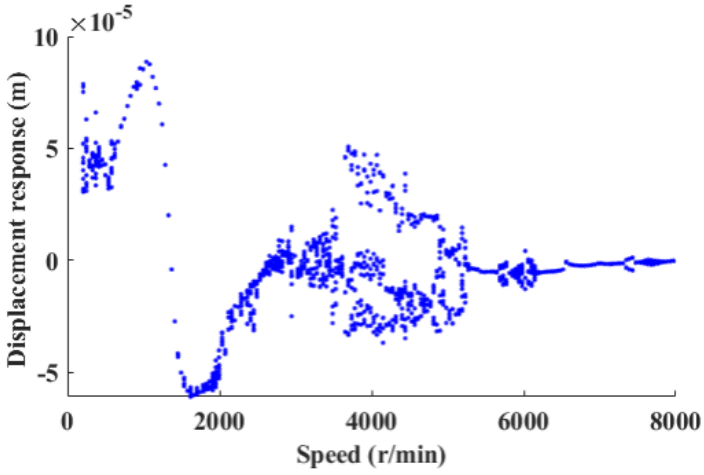

Figure 9. Bifurcation diagram with coupling backlash.

Figures 7–9 present the bifurcation diagram of torsional displacement for the case

of only considering tooth backlash, not coupling tooth-bearing backlash and coupling tooth-bearing backlash. **Figures 7–9** indicate that with the speed increase, bifurcation diagram exhibits evident nonlinear behavior such as single-periodic, double-periodic and chaos. In particular, the increased speed leads to the variation from periodic motion to chaotic motion.

Compared with only tooth backlash case, there are some newly emerging periodic and chaotic motion for not coupling backlash case, as shown in **Figure 8**. For example, with the speed increase, the gear system goes through a chaotic motion within the range of 400 r/min. Subsequently, it maintain a single periodic-one motion. The gear system enters a chaotic motion until input speed is up to 2600 r/min. It is observed that the only tooth backlash case exhibits a variation from chaotic motion to periodic motion around 6100 r/min. Until 7200 r/min, the gear system enters double-periodic interval. After going through chaotic motion in a small speed range, the gear system enters periodic motion again. These characteristics indicates that the introduced bearing backlash leads to the delay. The gear system enters chaotic motion and the range is widened heavily. Additionally, the amplitude of torsional displacement is enlarged, which is primarily caused by bearing backlash.

Compared with coupling and not coupling backlash cases, depicted in **Figures 8** and **9** exhibit that the tendencies of bifurcation characteristic curves are consistent with each other. In other word, with the speed increase, they all go through periodic motion and afterwards enter chaotic motion again. However, it appears evident difference with respect to the bifurcation behaviors. For the coupling backlash case, the gear system enters periodic-three motion with input speed 3650 r/min–4200 r/min. However, the not coupling backlash case enters single-periodic motion. Simultaneously, the coupling backlash case goes through chaotic motion with input speed 4600 r/min–5200 r/min while the not coupling backlash case goes through periodic-three motion. The coupling backlash case enters chaotic motion around 1500 r/min while the not coupling backlash case is around 2500 r/min, illustrating that the gear system enters chaotic motion in advance. After introducing coupling bearing backlash, the amplitudes of torsional displacement shown in **Figure 9** are larger than those in **Figure 8**. Note that the torsional displacement peak abruptly appears approximately 2150r/min shown in **Figure 8**, which maybe caused by the “resonance effect”.

Actually, the tooth-bearing backlash can be regarded as a newly emerging excitation resource alike impact force [23–25]. That maybe the causation that displacement amplitude and chaotic motion are changed significantly.

4. Parametric effect studies

To clearly exhibit the nonlinear behavior of gear system considering coupling tooth-bearing backlash, the influence of speed condition, tooth backlash, TVMS and bearing stiffness on the response is investigated numerically. The time history responses, phase diagrams, amplitude-frequency spectra and Poincare maps of central components are smoothly employed to perform the periodic and chaotic motion simultaneously. The parametric studies are extremely significant for capturing the nonlinear behavior.

4.1. Speed condition effect

Rotational speed is a critical parameter that has great influence on the behavior of gear system. In this section, bifurcation diagrams with respect to various speed conditions are presented. The bifurcation diagrams of torsional vibration can be depicted through calculating the dynamic Equation (22) by utilizing MATLAB software. **Figure 10** indicates that with the speed increase, gear system shows distinct periodic and chaotic motion. To better perform the nonlinear behavior, the vibration responses are calculated and simulated here, as illustrated in **Figure 11**.

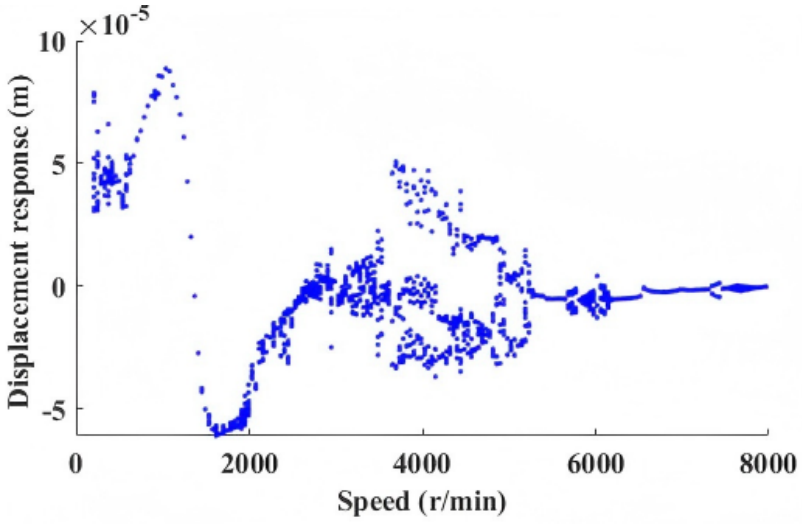

Figure 10. Variation of bifurcation diagram for different input speeds.

Figure 11 presents the nonlinear behavior of gear system with different input speeds, specifically 1000 rpm, 3000 rpm, 4000 rpm, 6000 rpm, 7400 rpm and 8000 rpm. The response curves illustrate that for input speed 1000 rpm, the gear system shows a typical periodic motion because the time history response presents a sine curve and the phase diagram presents a closed circle. Simultaneously, the amplitude-frequency spectra presents a single frequency while Poincare map presents a point. The above phenomena illustrate that the system with input speed 1000 rpm is in a stable condition. For input speeds 3000 rpm and 4000 rpm, the phase diagram presents a complex ellipse and Poincare map presents a disorder discrete point, illustrating that the gear system is in chaotic motion. For input speed 6000 rpm, the time history response presents a periodic sine curve while phase diagram and Poincare map present three ellipses and multiple points, revealing that the system is in a stable condition, i.e., periodic-three motion. For input speed 7400 rpm, the phase diagram presents regular curves with two closed ellipses and Poincare map two points, indicating that the system is in double-periodic motion. Ultimately, input speed 8000 rpm corresponds to distinct single-periodic motion.

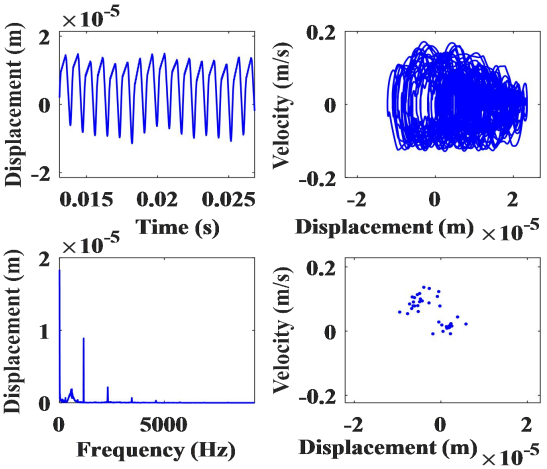

(**a**) Speed condition 1000 r/min

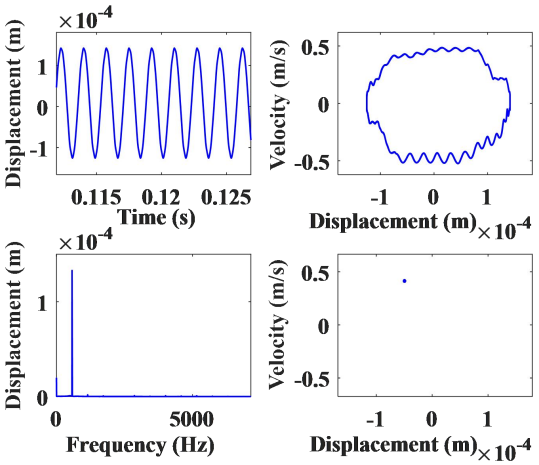

(**b**) Speed condition 3000 r/min

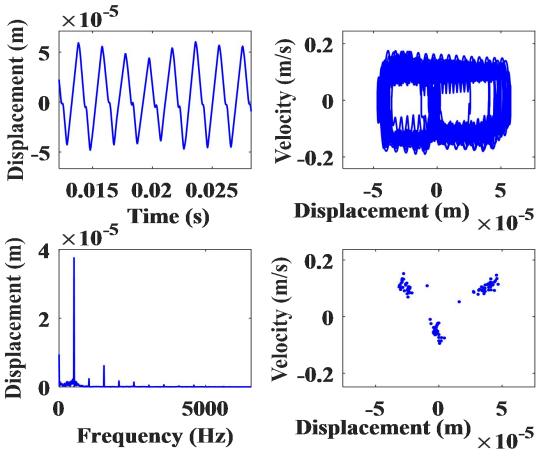

(**c**) Speed condition 4000 r/min

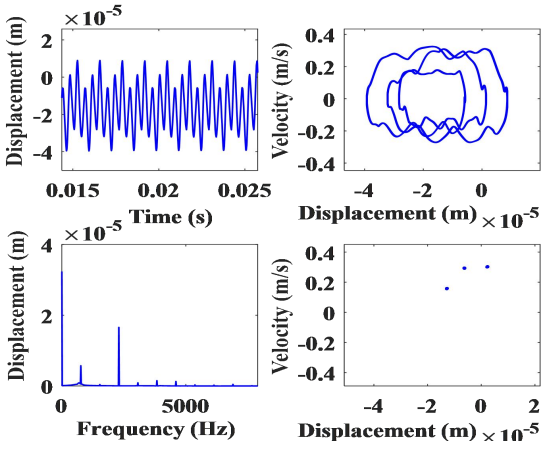

(**d**) Speed condition 6000 r/min

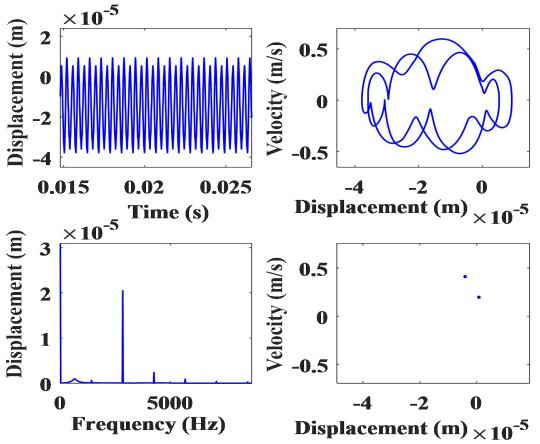

(**e**) Speed condition 7400 r/min

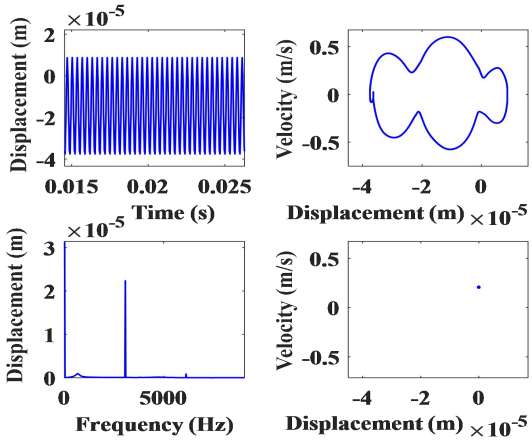

(**f**) Speed condition 8000 r/min

Figure 11. Response of gear transmission system for different speed condition.

To sum up, it is concluded that with the speed increasing, the gear transmission system exhibits significant single-periodic motion, double-periodic motion and chaos motion. The system with dynamic backlash induces double-periodic motion into chaotic motion. In order to make system operate smoothly, one should quickly pass the speed interval where large vibration is generated.

4.2. Dynamic backlash effect

The gear transmission system will occur teeth-contact, teeth-disengage and teeth-recontact while driving and driven gear are engaging with each other. Due to the dynamic backlash, the system performs strong nonlinearity and further affects the dynamic characteristic. **Figure 12** presents the bifurcation diagram of torsional displacement of gear system with input speed 4000 r/min. **Figure 12** indicates that with the parameter change, the original system undergoes periodic and chaotic motion. Bifurcation diagram also indicates single-periodic motion with backlash $b = 0.6$ um, double-periodic motion with $b = 1.8$ um and chaotic motion with $b = 3.0$ um. The above phenomenon indicates that dynamic backlash is a critical factor which determines the stability of the system. In order to significantly perform the nonlinear behavior, vibration response is further calculated and described in **Figure 13**.

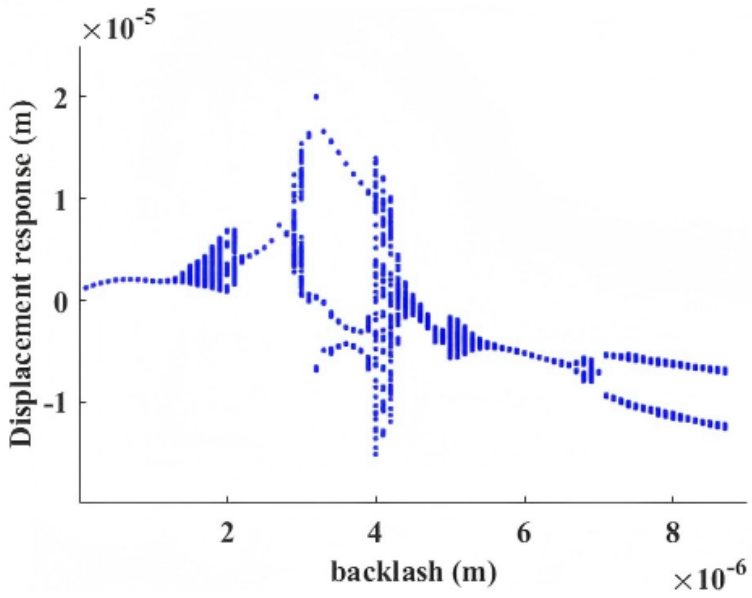

Figure 12. Variation of bifurcation diagram for different backlash parameters.

Figure 13 shows the variation of torsional response with respect to various backlash parameters 0.6 um, 1.8 um, 3.0 um, 4.0 um, 6.0 um, 8.0 um. Taking backlash parameter b = 6.0 um as example described in **Figure 13a** the system corresponding to single-periodic motion is described as (i) time history curve of gear system harmonic, (ii) phase diagram closed ellipse, (iii) Poincare map diagram only one point. For backlash case b = 8.0 um in **Figure 13b–d**, the system corresponding to quasi-periodic or chaotic motion is described as (i) time history curve complex harmonic curves, (ii) phase diagram complex disorder closed ellipse, (iii) Poincare map disorder closed discrete point. The motion states in **Figure 13e** are similar with those in **Figure 13a**. For backlash parameter b = 8.0 um in **Figure 13f**, the system corresponding to periodic-doubling motion is described as (i) time history curve harmonic, (ii) phase diagram two closed ellipse, (iii) Poincare map only two points.

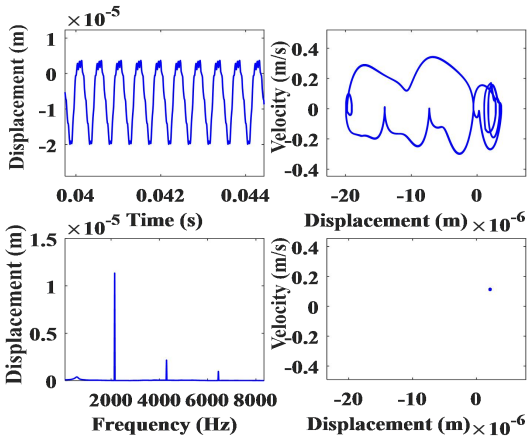

(**a**) Torsional response with backlash 0.6 um

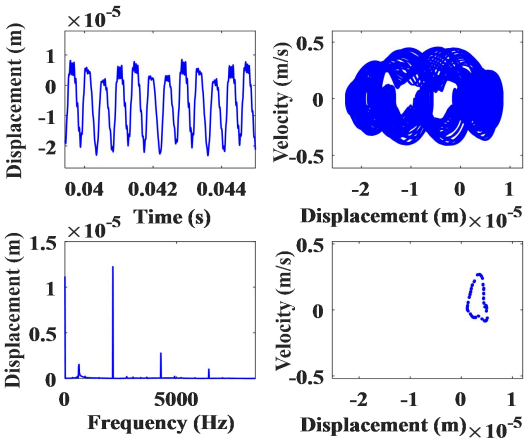

(**b**) Torsional response with backlash 1.8 um

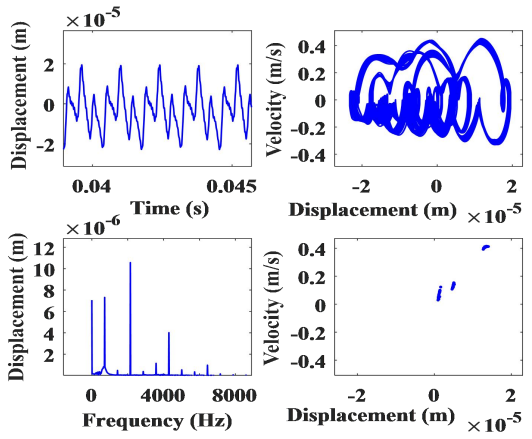

(**c**) Torsional response with backlash 3.0 um

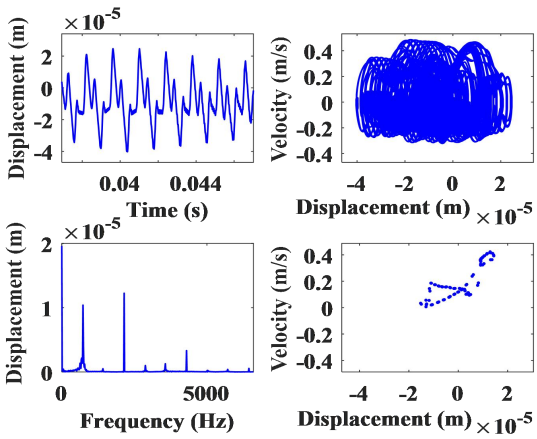

(**d**) Torsional response with backlash 4.0 um

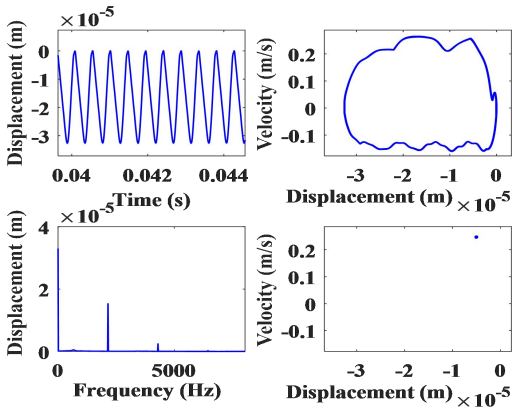

(**e**) Torsional response with backlash 6.0 um

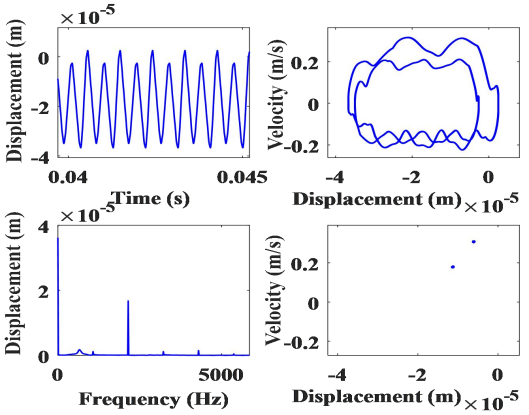

(**f**) Torsional response with backlash 8.0 um

Figure 13. Variation of torsional response for different backlash parameters.

In summary, the above studies illustrate that gear system exhibits periodic motion for small backlash. However, gear system will exhibit quasi-periodic or chaotic motion for large backlash. Selecting clearance parameter reasonably can diminish the large vibration corresponding to chaotic motion.

4.3. TVMS effect

Similar to the investigation on the influence of backlash, TVMS is also emphasized here. In this section, TVMS is selected as $K_m = sK_m(t)$ and its coefficient is $0.01 \leq s \leq$

10. The variation of bifurcation diagram for different TVMS is depicted by employing MATLAB software, as shown in **Figure 14**.

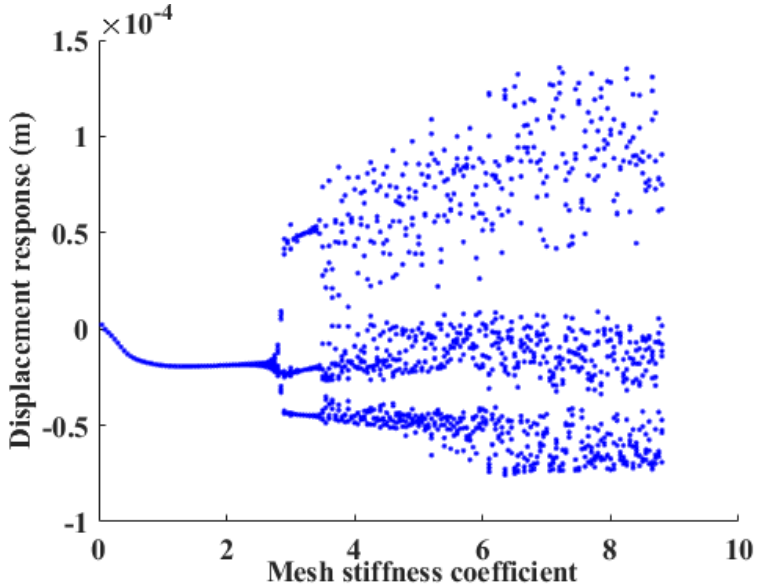

Figure 14. Bifurcation diagram for different meshing stiffness coefficients.

Figure 14 indicates that the gear system exhibits rich bifurcation behavior. The detailed variation process is described as follows. The dynamic system goes through a stable periodic-one motion for the case of $0 \leq s \leq 2.8$. Bifurcation varies from periodic-one motion to periodic-three motion while coefficient is selected as $0 \leq s \leq 2.8$. After maintaining periodic motion for a short process, bifurcation varies from periodic-three motion to an unstable chaotic motion again. Ultimately, the system is in an unstable and complex state of chaotic motion.

A further analysis is conducted to investigate the bifurcation behavior, as depicted in **Figure 15**. **Figure 15a** indicates that time history curve shows a significant sine or cosine characteristic. The phase diagram shows a single circle and the Poincare map shows a single point while stiffness coefficient satisfies $s = 1.0$. The phenomenon illustrates the gear system is in a state of periodic motion. **Figure 15b** indicates that phase diagram shows a closed ellipse with multiple winding and the Poincare map shows a "cloud like" discrete point corresponding to stiffness coefficient $s = 2.8$. **Figure 15c,d** indicate that the time history curves shows periodic sine or cosine curves. The phase diagram shows three closed circles while Poincare map shows three discrete points, which illustrates the gear system is in a state of chaotic motion. The motion states in **Figure 15e,f** are similar with those in **Figure 15b**.

To sum up, the above phenomenon illustrates that the bifurcation behavior varies with the stiffness coefficient increase. The system will in a state of single-periodic motion while meshing stiffness coefficient is very small. However, large meshing stiffness coefficient can cause the variation from periodic motion to chaotic motion. In order to realize the stable operation of system, one can prevent chao-induced damage by adjusting TVMS parameter reasonably.

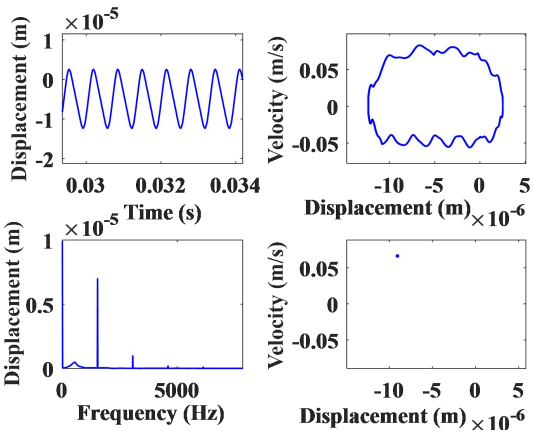

(**a**) Response with stiffness coefficient s = 1.0

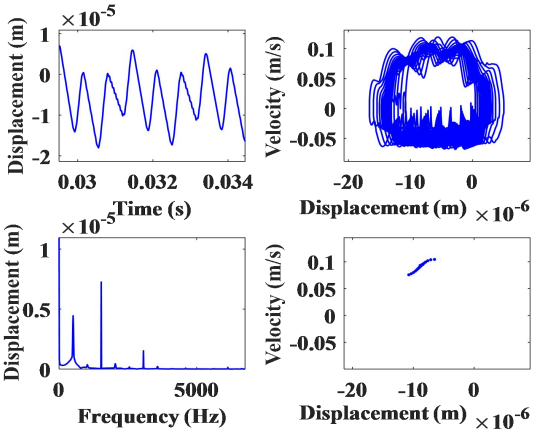

(**b**) Response with stiffness coefficient s = 2.8

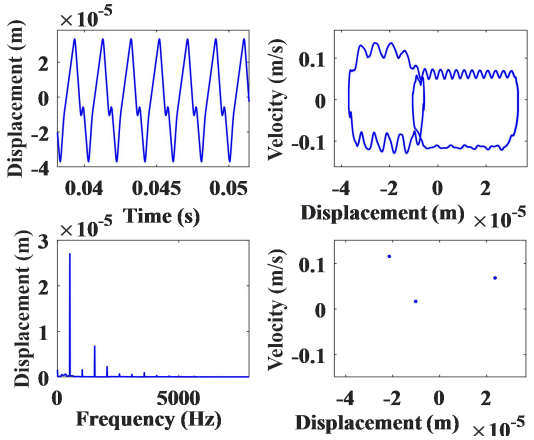

(**c**) Response with stiffness coefficient s = 3.2

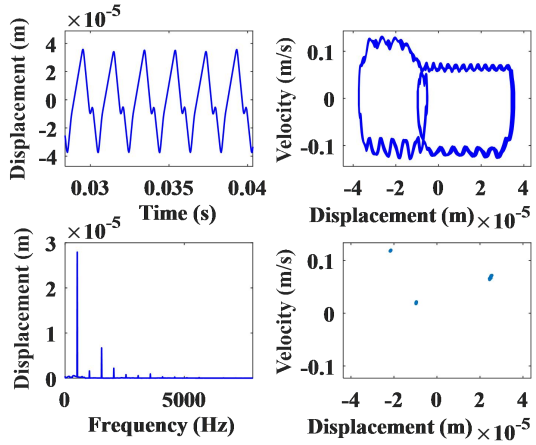

(**d**) Response with stiffness coefficient s = 3.4

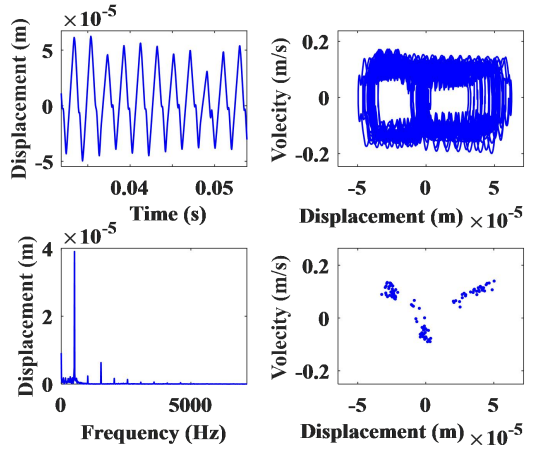

(**e**) Response with stiffness coefficient s = 6.0

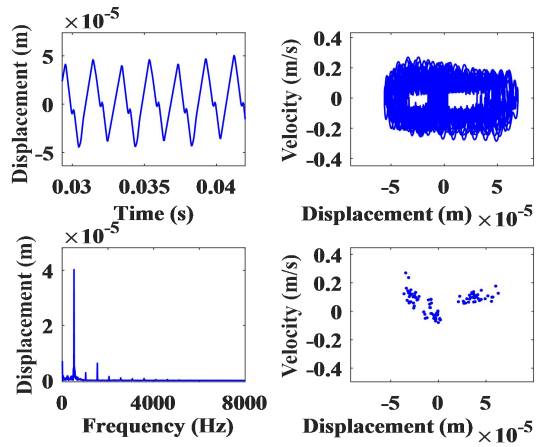

(**f**) Response with stiffness coefficient s = 8.0

Figure 15. Variation of torsional response for different meshing stiffness coefficients.

4.4. Bearing stiffness effect

In this section, the bearing stiffness is selected as $K_{s1} = rK_s$. Here, r is bearing stiffness coefficient and its range is $0.01 \leq r \leq 10$. The bifurcation diagram with different bearing stiffness coefficient can be simulated by employing MATLAB software. The bifurcation diagram is depicted in **Figure 16**, indicating a significant linear or nonlinear behavior, i.e., periodic motion and chaotic motion. The nonlinear behavior corresponding to different bearing stiffness coefficient is depicted

in **Figure 17**.

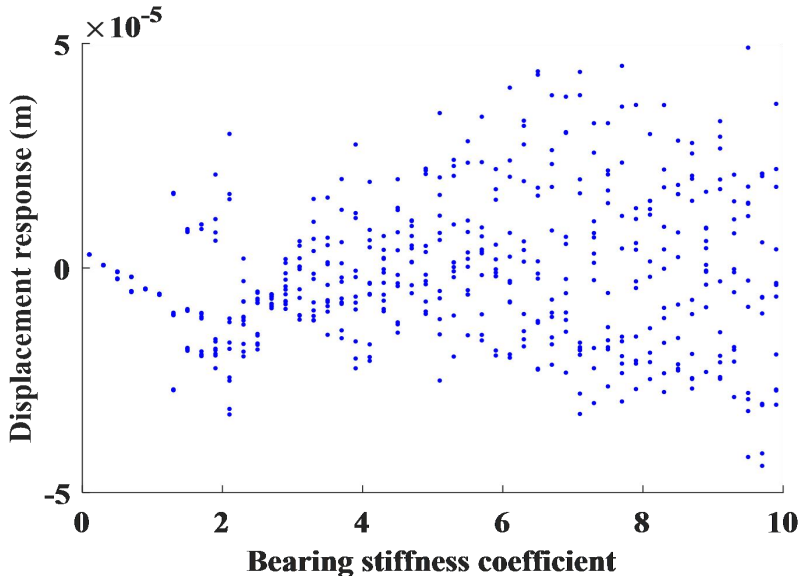

Figure 16. Bifurcation diagram for different bearing stiffness coefficients.

The gear system is a strongly nonlinear dynamic system. Similar research approach alike dynamic backlash and meshing stiffness can be employed to investigate the influence of bearing stiffness on the time history, frequency spectrum, phase diagram and Poincare map, as shown in **Figure 17**. It can be observed that the system exhibits complex motion with bearing stiffness parameter increase. **Figure 17a** exhibits a tendency that the system enters a single-periodic motion corresponding to bearing stiffness coefficient s = 0.1. **Figure 17b** depicts that the system goes through double-periodic motion for the case of s = 0.5. **Figure 17c** shows a single-periodic motion for the case of s = 1.0. Additionally, **Figure 17d–f** exhibit that the system is in a chaotic motion with respect to bearing stiffness coefficient s = 2.0, 4.0 and 8.0.

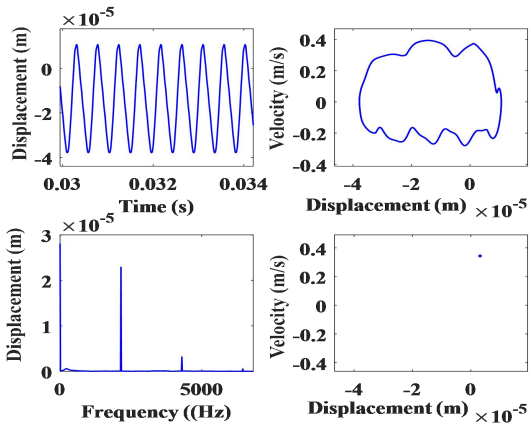

(**a**) Response with stiffness coefficient s = 0.1

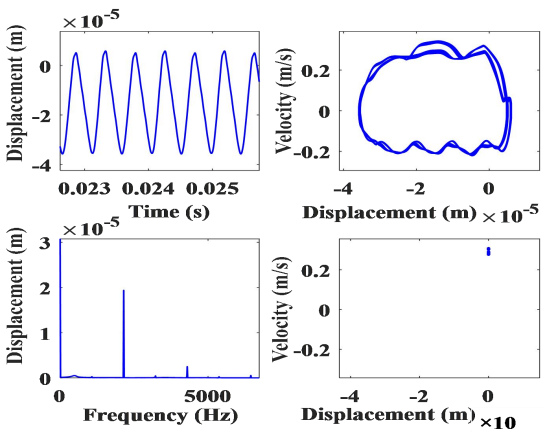

(**b**) Response with stiffness coefficient s = 0.5

Figure 17. *Cont.*

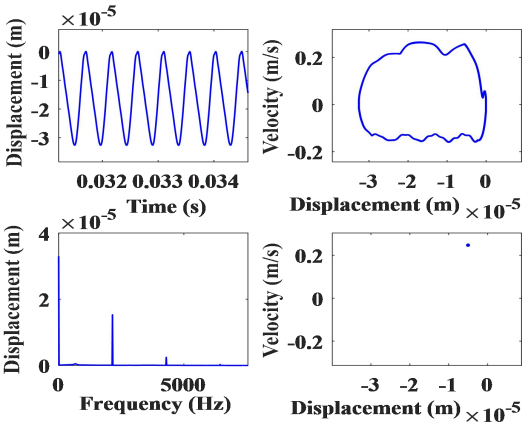

(**c**) Response with stiffness coefficient s = 1.0

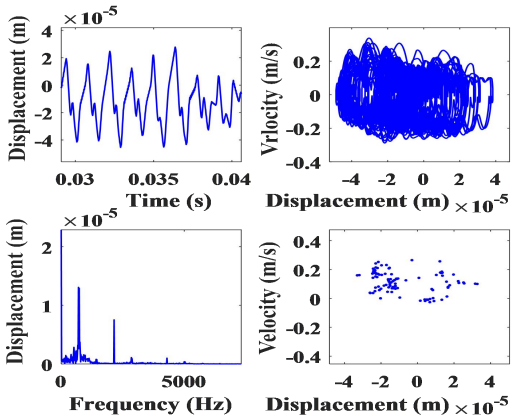

(**d**) Response with stiffness coefficient s = 2.0

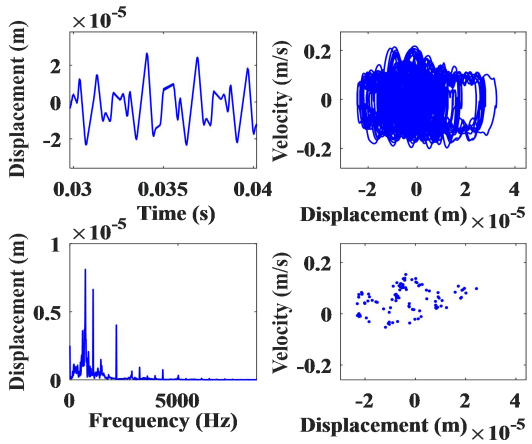

(**e**) Response with stiffness coefficient s = 4.0

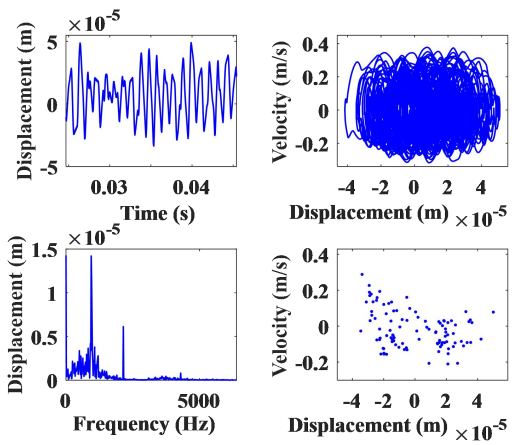

(**f**) Response with stiffness coefficient s = 8.0

Figure 17. Variation of torsional response for different bearing stiffness coefficients.

Figure 18 presents the variation of bifurcation behavior for different radial and axial bearing stiffness. It is observed that the two cases go through periodic and chaotic motion. The maximum displacement of radial case is larger than the axial case, illustrating that radial bearing stiffness has larger influence on the dynamic response. It is evident that bearing stiffness is also a primary reason causing the vibration amplification change.

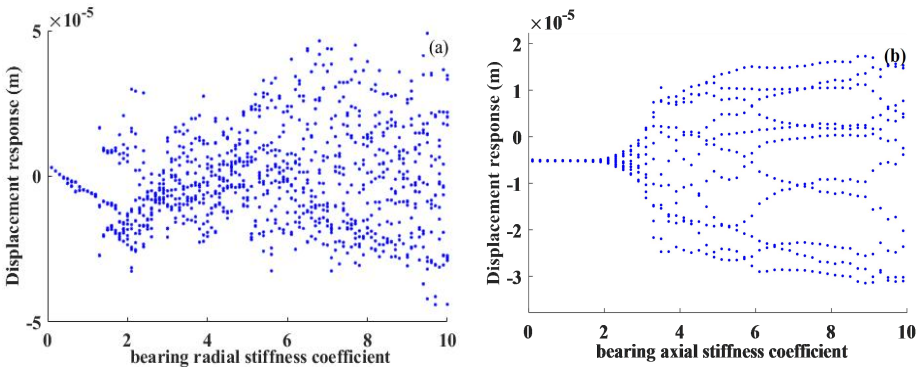

Figure 18. Variation of bifurcation behavior for different radial and axial bearing stiffness.

5. Conclusions

In this work, a novel nonlinear gear-shaft-bearing model considering tooth-bearing backlash and TVMS is developed through employing shafting element method. TVMS formula associated with tooth-bearing backlash is derived. Nonlinear behaviors of gear-shaft-bearing system are investigated. Several beneficial conclusions can be drawn:

(1) Tooth-bearing backlash are the strongly nonlinear factors. Compared with single backlash case, the displacement magnitude of gear-shaft-bearing system considering tooth-bearing backlash is enlarged due to the coupling effect.
(2) After considering the coupling effect, the nonlinear behavior such as time history, frequency spectrum, phase diagram and Poincare maps becomes more complex, indicating that the coupling backlash has more strong nonlinearity.
(3) The results also show that speed condition, TVMS and dynamic backlash can significantly affect the bifurcation diagram, periodic motion and chaotic motion.

Author contributions: Conceptualization, WL and YC; methodology, QW; software, HC; validation, HC and WD; formal analysis, WL, YC and HC; investigation, WD; resources, WD; data curation, HC; writing—original draft preparation, WL and QW; writing—review and editing, WL. All authors have read and agreed to the published version of the manuscript.

Funding: This work was supported by the Fundamental Research Funds for the Provincial Undergraduate Universities of Heilongjiang Province (Grant No. 2025BJ08), Natural Science Foundation of Heilongjiang Province (Grant No. PL2024E029) and Longjiang Project Young Goose Innovation Team Support Program (Grant No. 2024CYLJ02).

Conflict of interest: We declare that we have no conflict of interest.

References

1. Mélot A, Benaïcha Y, Rigaud E, et al. Effect of gear topology discontinuities on the nonlinear dynamic response of a multi-degree-of-freedom gear train. Journal of Sound and Vibration. 2022; 516: 116495. doi: 10.1016/j.jsv.2021.116495
2. Debeurre M, Grolet A, Cochelin B, et al. Finite element computation of nonlinear modes and frequency response of geometrically exact beam structures. Journal of Sound and Vibration. 2023; 548: 117534. doi: 10.1016/j.jsv.2022.117534
3. Ning Z, Bai Z. Nonlinear dynamics of space manipulator system considering planetary gear joints. Mechanism and Machine Theory. 2025; 214: 106136. doi: 10.1016/j.mechmachtheory.2025.106136
4. Pizzolante F, Battarra M, Mucchi E, et al. Combining the asymptotic numerical method with the harmonic balance method to capture the nonlinear dynamics of spur gears. Mechanical Systems and Signal Processing. 2024; 214: 111384. doi: 10.1016/j.ymssp.2024.111384
5. Cao Y, Yao H, Li H, et al. Torsional vibration dynamics of a gear-shafting system attaching a nonlinear energy sink. Mechanical Systems and Signal Processing. 2022; 176: 109172. doi: 10.1016/j.ymssp.2022.109172
6. Ren Z, Li J, Wang K, et al. Nonlinear dynamic analysis of a coupled lateral-torsional spur gear with eccentricity. Journal of Vibroengineering. 2016; 18(7): 4776–4791. doi: 10.21595/jve.2016.17067
7. Hu Y-H, Du Q-G, Xie S-H. Nonlinear dynamic modeling and analysis of spur gears considering uncertain interval shaft misalignment with multiple degrees of freedom. Mechanical Systems and Signal Processing. 2023; 193: 110261. doi: 10.1016/j.ymssp.2023.110261

8. Wei J, Zhang A, Wang G, et al. A study of nonlinear excitation modeling of helical gears with Modification: Theoretical analysis and experiments. Mechanism and Machine Theory. 2018; 128: 314–335. doi: 10.1016/j.mechmachtheory.2018.06.005
9. Shi J, Gou X, Jin W, et al. Multi-meshing-state and disengaging-proportion analyses of a gear-bearing system considering deterministic-random excitation based on nonlinear dynamics. Journal of Sound and Vibration. 2023; 544: 117360. doi: 10.1016/j.jsv.2022.117360
10. Xiang L, Zhang Y, Gao N, et al. Nonlinear dynamics of a multistage gear transmission system with multi-clearance. International Journal of Bifurcation and Chaos. 2018; 28(03): 1850034. doi: 10.1142/S0218127418500347
11. Pan W, Li X, Wang L, et al. Nonlinear response analysis of gear-shaft-bearing system considering tooth contact temperature and random excitations. Applied Mathematical Modelling. 2019; 68: 113–136. doi: 10.1016/j.apm.2018.10.022
12. Zhang HB, Wang R, Chen ZK, et al. Nonlinear dynamic analysis of a gear-rotor system with coupled multi-clearance. Journal of Vibration and Shock. 2015; 34: 144–150. Available online: https://jvs.sjtu.edu.cn/EN/Y2015/V34/I8/144
13. Aihara T, Sakamoto K. Theoretical analysis of nonlinear vibration characteristics of gear pair with shafts. Theoretical and Applied Mechanics Letters. 2022; 12(2): 100324. doi: 10.1016/j.taml.2022.100324
14. Wang S, Zhu R. Nonlinear dynamic analysis of GTF gearbox under friction excitation with vibration characteristics recognition and control in frequency domain. Mechanical Systems and Signal Processing. 2021; 151: 107373. doi: 10.1016/j.ymssp.2020.107373
15. Sun Z, Chen S, Hu Z, et al. Vibration response analysis of a gear-rotor-bearing system considering steady-state temperature. Nonlinear Dynamics. 2022; 107(1): 477–493. doi: 10.1007/s11071-021-07024-8
16. Gill-Jeong C. Analysis of the nonlinear behavior of gear pairs considering hydrodynamic lubrication and sliding friction. Journal of Mechanical Science and Technology. 2009; 23(8): 2125–2137. doi: 10.1007/s12206-009-0623-x
17. Lu CR, Li YN, Dou ZC, et al. Nonlinear vibration characteristics of bending torsional coupling of gear rotor-bearing system. Journal of Vibration engineering. 2018; 31: 238–244.
18. Liu W, Shi K, Tupolev V, et al. Nonlinear dynamics of a two-stage planetary gear system with sliding friction and elastic continuum ring gear. Journal of Mechanical Science and Technology. 2022; 36(1): 77–85. doi: 10.1007/s12206-021-1206-8
19. Chen B, Cui Z, Jiang H. Producing negative active stiffness in redundantly actuated planar rotational parallel mechanisms. Mechanism and Machine Theory. 2018; 128: 336–348. doi: 10.1016/j.mechmachtheory.2018.06.002
20. David BS. Geared rotor dynamic methodologies for advancing prognostic modeling capabilities in rotary-wing transmission systems [PhD thesis]. University of Virginia; 2008. Available online: https://www.proquest.com/docview/304438408
21. Huang K, Yi Y, Xiong Y, et al. Nonlinear dynamics analysis of high contact ratio gears system with multiple clearances. Journal of the Brazilian Society of Mechanical Sciences and Engineering. 2020; 42(2): 98. doi: 10.1007/s40430-020-2190-0
22. Cai Y. Simulation on the rotational vibration of helical gears in consideration of the tooth separation phenomenon (a new stiffness function of helical involute tooth pair). Journal of Mechanical Design. 1995; 117(3): 460–469. doi: 10.1115/1.2826701
23. Xiang L, Gao N, Hu A. Dynamic analysis of a planetary gear system with multiple nonlinear parameters. Journal of Computational and Applied Mathematics. 2018; 327: 325–340. doi: 10.1016/j.cam.2017.06.021
24. Wang J, Wu Z, Wang H, et al. Analysis of influence of thermal tooth backlash on nonlinear dynamic characteristics of planetary gear system. Nonlinear Dynamics. 2025; 113(1): 289–311. doi: 10.1007/s11071-024-10160-6
25. Mo S, Wang Z, Tang X, et al. Nonlinear dynamics of planetary gearboxes containing cracks. Nonlinear Dynamics. 2024; 112(19): 17007–17031. doi: 10.1007/s11071-024-09942-9